Modeling Directional Brightness Temperature Over Mixed Scenes of Continuous Crop and Road: A Case Study of the Heihe River Basin

Biao Cao, Qinhuo Liu, Yongming Du, Hua Li, Heshun Wang, and Qin Xiao

***Abstract*—A new geometric optical model is proposed in this letter to simulate the directional brightness temperature (DBT) distribution over mixed scenes of continuous crop and road. The DBT distributions of the crop and road zones are separately calculated, and the road zone consists of a road and adjacent crop sides. A road distribution polar map is designed to show all of the roads of different lengths, widths, and orientations in the scene. The airborne multiangle data set of the thermal infrared band that was acquired during the Heihe Watershed Allied Telemetry Experimental Research experiment is used for validation. The results demonstrate that the proposed model can simulate the DBT of a heterogeneous scene (90×90 m^2) with a root-mean-square error equal to 1.1 K and good trend similarity.**

***Index Terms*—Directional brightness temperature (DBT), geometric optical model, Heihe Watershed Allied Telemetry Experimental Research (HiWATER), heterogeneous, multiangle.**

I. Introduction

THE land surface temperature (LST) is one of the most important parameters in the physical processes of surface energy and water balance at both the local and global scales [1]. Remote sensing products offer the only possibility of measuring LST with complete spatially averaged values [2].

LST retrieval from remote sensing faces three main difficulties: atmospheric correction, temperature and emissivity separation, and thermal radiation directionality. Some practical algorithms have been proposed and applied to address the first two issues [3]. However, the problem of thermal radiation directionality has not been considered in any satellite LST product. This unsolved problem brings significant uncertainty to the subsequent application.

Many models have been proposed since the 1960s to simulate the directional brightness temperature (DBT) distribution over different underlying surfaces. The underlying surfaces, such as vegetation, bare soil, urban, snow, and water, have been widely discussed [4]–[7]. However, a remote sensing pixel usually consists of a variety of surface types. The contradiction between the model assumption (homogeneous) and the land surface status (heterogeneous) results in the lack of consideration of the thermal radiation directionality problem in the current operational LST products.

There are many models to simulate the DBT distribution of crop scenes during different growth stages. These models can obtain good validation results if the camera is mounted on the beam of a crane or a portable multiangle observation system (the footprint is approximately several meters). However, it is difficult to obtain satisfactory results for applications in satellite pixel scales (the pixel resolution is approximately hundreds or thousands of meters). The endmembers of noncrops within a satellite pixel decrease the accuracy of these models. In addition to the effect of continuous crops, we attempted to build a new DBT model that considers the effect of the road. This model is referred to as CCM. The spatial scale of the CCM is approximately 100 m (corresponding to the resolutions of the thermal infrared (TIR) band of Advanced Spaceborne Thermal Emission and Reflection Radiometer (ASTER) and TM8) because a larger region may contain other land covers, such as houses, water, and forest.

Section II introduces the experimental data. A detailed description of CCM is given in Section III. The modeled DBT results and validation results that were extracted from the airborne data are analyzed in Section IV. The sensitivity analysis and the conclusion are given in Sections V and VI, respectively.

II. Experimental Data

A. HiWATER Experiment

Heihe Watershed Allied Telemetry Experimental Research (HiWATER) is an ongoing watershed-scale ecohydrological experiment designed from an interdisciplinary perspective to address problems that include the heterogeneity, scaling, uncertainty, and closing of the water cycle at the watershed scale [8]. This experiment was performed in the Heihe river basin in the arid region of northwest China (Gansu Province).

B. Ground Site

The field observations and airborne data that were used in this study were derived from the key experimental areas of the middle reaches. The location and land coverage of the study area are presented in Fig. 1. The scene consists of crops (maize) and roads. The longitude (latitude) of the center point of this study area is 100.37313 E and 38.85845 N. The size of this area is 90×90 m^2, corresponding to the spatial resolution of the TIR band of ASTER.

Manuscript received January 30, 2014; revised May 5, 2014; accepted May 24, 2014. This work was supported in part by the National Basic Research Program of China under Grant 2013CB733401 and in part by the National Natural Science Foundation of China under Grant 91125003, Grant 41171282, and Grant 41101325.

The authors are with the State Key Laboratory of Remote Sensing Science, Institute of Remote Sensing and Digital Earth of Chinese Academy of Sciences, Beijing 100101, China, and also with the University of Chinese Academy of Sciences, Beijing 100049, China (e-mail: duym@irsa.ac.cn).

Color versions of one or more of the figures in this paper are available online at http://ieeexplore.ieee.org.

Digital Object Identifier 10.1109/LGRS.2014.2333874

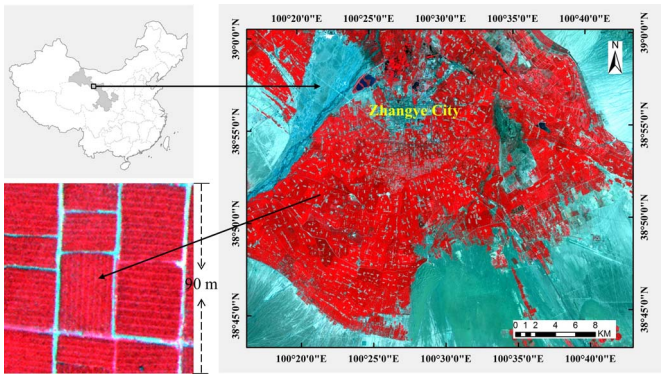

Fig. 1. Location and land coverage of the study area.

Fig. 2. Measurements of 15 parallel flight tracks.

C. WiDAS Instrument and Flight Protocol

The Wide-angle Infrared Dual-mode line/area Array Scanner (WiDAS) is one of the major instruments that were used in the airborne missions [8]. A thermal infrared camera, i.e., FLIR A655sc, was equipped with $68^\circ \times 54^\circ$ wide-angle field-of-view lens and was placed aboard the aircraft with a forward inclination of 12°. The camera provided 640×480 pixel images. The aircraft speed was 200 km/h, and the image acquisition rate was 6 images/s. The flights were conducted at a height about 1.16 km above ground level.

The flight protocol consisted of several long parallel flight lines that were flown in opposite directions, as shown in Fig. 2. One track in one direction took about 4 min, and the turning took about 4 min. The flight experiment began at the local time of 10:36 (Track 15) and finished at 14:14 (Track 1) on August 3, 2012 [9].

The overlap between two sequential WiDAS images is greater than 85% in the TIR band, indicating that the same ground point can be almost simultaneously observed in several sequential images. We extracted 15 observations with different view angles (from -50° to $+20^\circ$, step $= 5^\circ$) in one track.

After calibration, lens distortion correction, geometric correction, viewing angle retrieval, and atmospheric correction, the multiangle data set was built. The spatial resolution of the TIR band was resampled to 5 m after the preprocessing steps. Therefore, the patch size of this study area in the TIR images was 18×18.

D. Canopy Structure Parameters and Component Brightness Temperatures

The average canopy height of this study area was 2.1 m, which was measured by tapeline. The leaf area index (LAI) and the mean leaf angle (MLA) were 3.6 and 52°, respectively, as measured by LAI-2000. The component brightness temperature was measured by a Fluke thermal radiometer (8–14 μm). The radiometer was calibrated using a Mikron M340 blackbody within a temperature range of $0^\circ - 60^\circ$. The calibrated component brightness temperatures are shown in Table I.

TABLE I
BRIGHTNESS TEMPERATURES OF SIX COMPONENTS (K)

Sunlit soil	Shaded soil	Sunlit leaf	Shaded leaf	Sunlit road	Shaded road
304.9	299.7	302.4	300.3	316.7	300.4

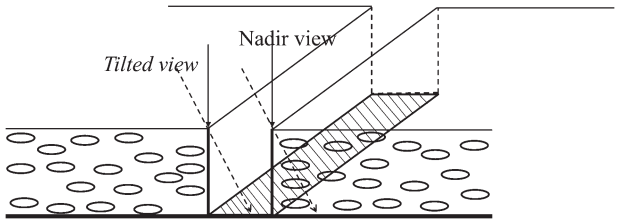

Fig. 3. Three-dimensional view of the crop zone and the road zone. The soil, leaf, and road components are illustrated by the bold solid line, black ellipses, and striped parallelogram, respectively. The crop zone consists of the leaf and the soil. The road zone consists of the road and the adjacent crop sides (shown as a letter "U" in the 2-D view of the profile).

III. METHODOLOGY

A. Modeling Over Mixed Scenes of Continuous Crop and Road

The scene is initially divided into two zones: a crop zone and a road zone (see Fig. 3). The road zone consists of a road and the adjacent crop sides. The internal components of the road zone are the sunlit road, shaded road, sunlit side, and shaded side. The internal components of the crop zone are the sunlit soil, shaded soil, sunlit leaf, and shaded leaf.

The road will be obstructed by the crop side in the tilted observation direction. However, the crop side is incorporated into the road zone. Therefore, the obstruction only changes the proportions of the internal components of the road zone while maintaining the proportion of the road zone.

The sensor-received signal is the sum of the two zones weighted by the area proportions in this direction. The radiance of the crop and road zones can be calculated using the corresponding submodels (see Sections III-C and III-D).

It is difficult to discuss the directional radiometric temperature distribution of nonisothermal surfaces [4]–[6]. In this study, we attempt to model the DBT angular variation. The relationship between the DBT of the mixed scene and the six component brightness temperatures can be expressed as

$$T_B(\theta,\varphi) = \left[P_{\text{crop}}(\theta,\varphi) \cdot \sum_{i,j} f_{i,j}(\theta,\varphi) T_{i,j}^4 + P_{\text{road}}(\theta,\varphi) \cdot \sum_{i,k} F_{i,k}(\theta,\varphi) T_{i,k}^4 \right]^{\frac{1}{4}}, \quad (1)$$

$$i = \text{sunlit,shaded};\ j = \text{soil,leaf};\ k = \text{road,leaf}$$

where $T_B(\theta,\varphi)$ is the DBT of the mixed scene; $P_{\text{crop}}(\theta,\varphi)$ and $P_{\text{road}}(\theta,\varphi)$ are the overall fraction of each zone, with a sum equal to 1; $f_{i,j}(\theta,\varphi)$ and $T_{i,j}$ are the internal component

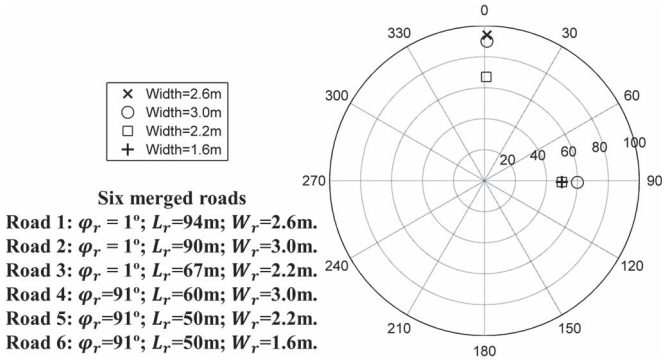

Fig. 4. Polar map of the roads within the case study area. The radii correspond to the road direction, and the concentric circles indicate the road length. The symbol types correspond to the road width.

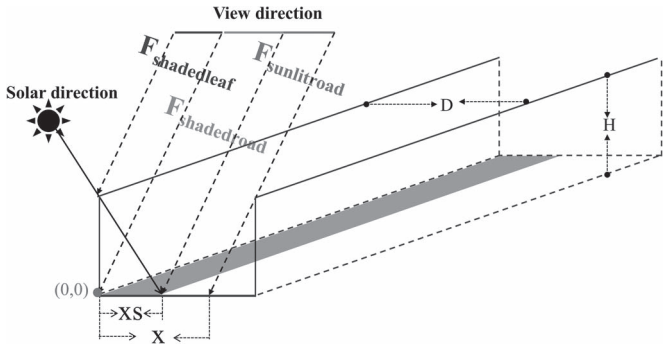

Fig. 5. Four components (sunlit road, shaded road, sunlit side, and shaded side) can be observed. The crop side is assumed to be opaque as Kimes' box model, meaning that no soil can be observed in the road zone.

fractions and brightness temperatures of the crop zone, respectively; and $F_{i,k}(\theta,\varphi)$ and $T_{i,k}$ are the internal component fractions and brightness temperatures of the road zone, respectively. Here, we do not consider the brightness temperature directionality of the six components.

B. Road Distribution Parameterization

A road has three features: direction (φ_r), length (L_r), and width (W_r). We propose to show all of the features of all of the roads within the case study area using a polar map, as shown in Fig. 4. There are only six points in Fig. 4 because the roads with the same width and the same direction are merged.

$P_{\mathrm{road}}(\theta,\varphi)$ and $P_{\mathrm{crop}}(\theta,\varphi)$ can be calculated based on the polar map information using

$$P_{\mathrm{road}}(\theta,\varphi)=\sum_{\varphi_r=0}^{\varphi_r=\pi}\frac{W_r\cdot L_r}{\mathrm{Area}_{\mathrm{total}}} \tag{2}$$

$$P_{\mathrm{crop}}(\theta,\varphi)=1-P_{\mathrm{road}}(\theta,\varphi). \tag{3}$$

C. DBT Model of the Crop Zone

It can be observed in Fig. 1 that the ridges within the crop zone are almost covered by leaves. The 4SAIL model that was developed by Verhoef *et al.* [10] is aimed at this uniform scene; however, this model cannot output the component proportions $f_{i,j}(\theta,\varphi)$. Fortunately, Yan *et al.* [11] proposed a method to calculate the component proportions of the crop zone. The inputs of this methods are the solar zenith angle (SZA), the solar azimuth angle, the view zenith angle (VZA), the view azimuth angle, leaf area angle (LAI), clumping index (λ), canopy height (H), leaf size factor (d), and G value. λ is equal to 1 for the uniform canopy. d is determined by the leaf shape [see (4)]. The maize leaf can be equivalent to a rectangle with a $\mathrm{Leaf}_{\mathrm{length}}$ equal to 0.5 m and a $\mathrm{Leaf}_{\mathrm{width}}$ equal to 0.087 m. Therefore, d is equal to 0.21 ($c=1$, for rectangle leaves). G value is determined by the leaf angle distribution (LAD). Here, the G value remains equal to 0.5 because the spherical LAD (MLA $=57.5^\circ$) is adopted to replace the real LAD (MLA $=52^\circ$) with a root-mean-square error (RMSE) of less than 0.03.

$$d=c\cdot\sqrt{\mathrm{Leaf}_{\mathrm{length}}\cdot\mathrm{Leaf}_{\mathrm{width}}} \tag{4}$$

D. DBT Model of the Road Zone

The box structure model that was developed by Kimes [12] can help us calculate the four component fractions $F_{i,k}(\theta,\varphi)$ under different geometric conditions. Here, we assume that the crop side is opaque as Kimes' box model (see Fig. 5). The basic structure of the box model is a soil ridge and a vegetation row, but the basic structure of the road zone model is a road ridge and two adjacent sides, which is the critical difference between Kimes' box model and the road zone model of this letter.

TABLE II
PROPORTIONS OF THE FOUR COMPONENTS OF ONE ROAD ZONE

xs	*x*	$F_{sunlitleaf}$	$F_{shadedleaf}$	$F_{sunlitroad}$	$F_{shadedroad}$
when the sensor is in the nadir direction					
0<xs<D	x=0	0	0	*(D-xs)/D*	*xs/D*
xs>D	*x=0*	0	0	0	1
when the sensor is on the opposite side of the solar direction					
0<xs<D	*xs<x<D*	0	*(D-x)/D*	*(x-xs)/D*	*xs/D*
0<xs<D	*0<x<xs*	0	*(D-x)/D*	0	*x/D*
0<xs<D	*x<0*	0	1	0	0
xs>D	*0<x<D*	0	*(D-x)/D*	0	*x/D*
xs>D	*x<0*	0	1	0	0
when the sensor is on the same side as the solar direction					
0<xs<D	*x>D*	1	0	0	0
0<xs<D	*xs<x<D*	*x/D*	0	*(D-x)/D*	*0*
0<xs<D	*0<x<xs*	*x/D*	0	*(D-xs)/D*	*(xs-x)/D*
xs>D	*xs>x*	1	0	0	0
xs>D	*D<x<xs*	$\frac{\tan\theta_{vr}}{\tan\theta_{sr}}$	1-$F_{sunlitleaf}$	0	0
xs>D	*x<D*	$\frac{\tan\theta_{vr}}{\tan\theta_{sr}}$	*x/D*-$F_{shadedleaf}$	0	*(D-x)/D*

The first step is transforming the VZA and the SZA to the view row angle and the solar row angle using

$$\tan\theta_{\mathrm{vr}}=\tan\theta_v\cdot\left|\cos\left(\varphi_v+\frac{\pi}{2}-\varphi_r\right)\right| \tag{5}$$

$$\tan\theta_{\mathrm{sr}}=\tan\theta_s\cdot\left|\cos\left(\varphi_s+\frac{\pi}{2}-\varphi_r\right)\right|. \tag{6}$$

The second step is calculating the relative horizontal distance of the intersection point of view (or solar) vector with the ground [see x (or xs) in Fig. 5].

The third step is calculating the proportions $(F_{r,i,k}(\theta,\varphi))$ of the four components of each road zone with different $x(xs)$ values. The results in different cases are summarized in Table II.

The final step is calculating $F_{i,k}(\theta,\varphi)$ through summing $F_{r,i,k}(\theta,\varphi)$ weighted by the ratio of each road area and the area of all of the roads using

$$F_{i,k}(\theta,\varphi)=\sum_{\varphi_r=0}^{\varphi_r=\pi}F_{r,i,k}(\theta,\varphi)\times\frac{W_r\cdot L_r}{P_{\mathrm{road}}(\theta,\varphi)\times\mathrm{Area}_{\mathrm{total}}}. \tag{7}$$

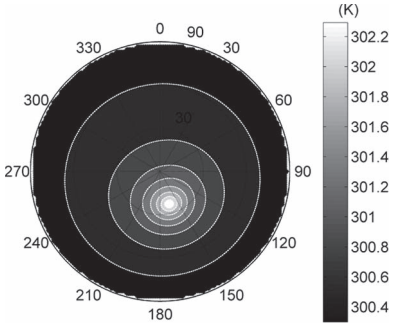

Fig. 6. DBT of the crop zone.

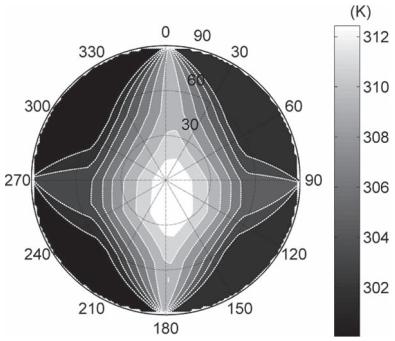

Fig. 7. DBT of the road zone.

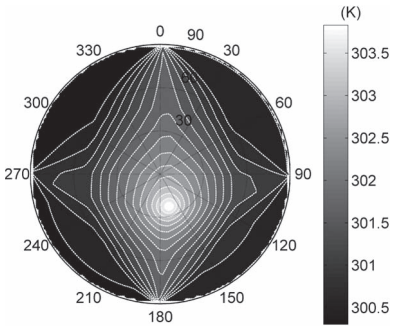

Fig. 8. DBT of the crop and road mixed scene.

IV. Case Study

A. Input Parameters

The input parameters of CCM include the architecture parameters of the crop zone (introduced in Sections II-D and III-C), the road information (see Fig. 4), and the six component brightness temperatures (see Table I).

B. Modeled DBT Distribution Over the Corn and Road Zones

Fig. 6 shows the DBT distribution of the crop zone. The concentric circles indicate the zenith view angles, and the radii correspond to the azimuth view angles. The DBT of the solar position ($\theta_s = 23.4^\circ$, $\varphi_s = 164.3^\circ$) is maximal because only the sunlit components can be observed in this direction [13].

Fig. 7 shows the DBT distribution of the road zone. Two series of concentric ovals can be clearly observed in this figure. Most of the road in the east–west direction is shaded by crops. Therefore, the feature brought by the roads in the east–west direction is suppressed, and that in the north–south direction is dominant.

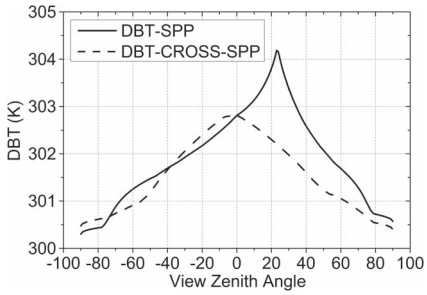

Fig. 9. DBT in the SPP and the cross-SPP.

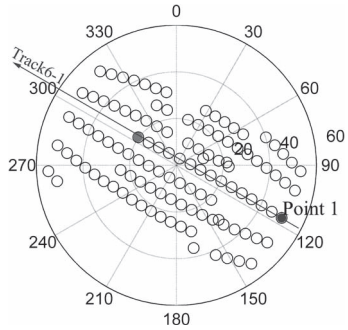

Fig. 10. All of the observations of this heterogeneous scene (90×90 m^2).

C. Modeled DBT Distribution Over the Mixed Scene

After simulating the DBT distributions of the crop and road zones, the DBT distribution of the mixed scene (see Fig. 8) can be calculated easily with the support of the proportions of the two zones in the nadir direction. The basic feature of the DBT of the mixed scene is similar to that of the road zone, although the road zone proportion is only equal to 0.127. The DBT feature around the hot spot is similar to that of the crop zone (see Fig. 6). Fig. 9 shows the DBT profiles in the solar principal plane (SPP) and the cross-SPP. The DBT difference between the solar position and the nadir position is 1.4 K.

D. Validation Using the DBT Profile Extracted From WiDAS

The study area can be observed in 115 points of all of the tracks (see Fig. 10). To avoid the uncertainty brought by the strong temporal fluctuation of multitracks, only the 15 view angles of the nearest track (track 6-1) were used for validation. The component brightness temperatures in Table I were measured during the flight time of track 6-1 (12:59 to 13:02).

As shown in Fig. 11, the simulated results of CCM are systematically underestimated compared with the observed results of WiDAS. The main sources of error include the error caused by ignoring the multiscatter effect within the crop zone, the camera calibration error, and the atmospheric correction error. The RMSE of the CCM is equal to 1.1 K for this site. The underestimated magnitude of the CCM is consistent with the conclusion of Chen and Liu that the multiscatter effect brings an approximately 0.8–1.3 K increase to the canopy DBT when the VZA is less than 50° and the soil and leaf temperatures are equal to 293 K [14].

The crop zone proportion of this study area is larger than 85%. Therefore, the 4SAIL model can be used for cross comparison. The inputs of 4SAIL are shown in Table III. The leaf and soil emissivities were measured using the ABB Bomem MR304 spectroradiometers. The modeled DBT results

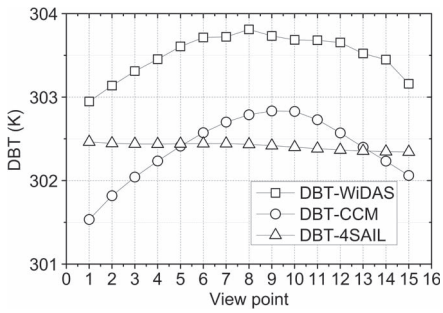

Fig. 11. DBT comparison in the 15 angles of track 6-1.

TABLE III
4SAIL INPUTS: COMPONENT RADIOMETRIC TEMPERATURES AND EMISSIVITIES

Sunlit soil	Shaded soil	Sunlit leaf	Shaded leaf	T_{Sky}	Leaf emissivity	Soil emissivity
307.3K	301.8K	303.7K	301.5K	258K	0.964	0.936

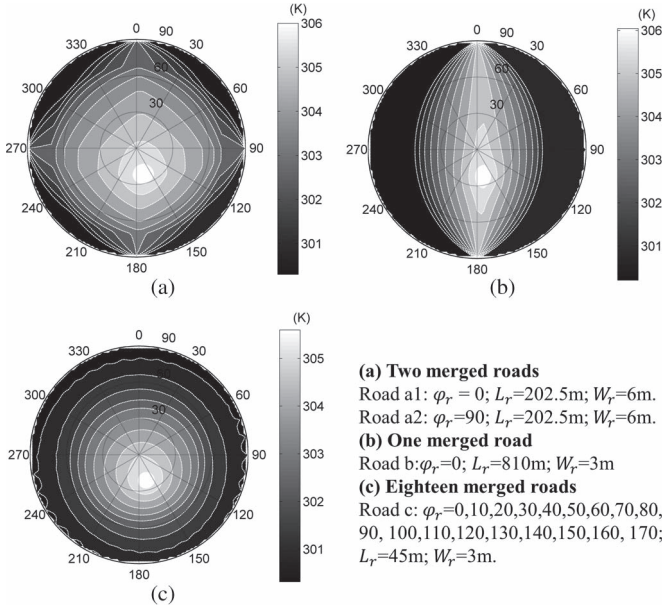

Fig. 12. DBT polar maps of three extreme cases.

of 4SAIL are underestimated (see Fig. 11) because the road zone was not considered. Although the RMSE of the 4SAIL results is equal to that of the CCM (also 1.1 K), we consider the CCM to be more suitable due to its higher similarity of trend.

V. SENSITIVITY ANALYSIS

The road parameters of three extreme cases are shown in Fig. 12. The input crop architecture parameters remain unchanged in the three extreme cases. The input component brightness temperatures remain unchanged in Fig. 12(a) and (c). The input brightness temperatures of the sunlit (shaded) soil in Fig. 12(b) are set to be equal to that of the sunlit (shaded) road to correspond to the row-planted model. The maximum DBT values in Fig. 12(a)–(c) are higher than those in Fig. 8 because the P_{road} values in Fig. 12(a)–(c) are all equal to 0.3 (>0.127 than those in Fig. 8).

It can be observed in Fig. 12(a) that the enlarged road width leads to an increase in the short semiaxis length of the concentric ovals. Fig. 12(b) confirms the simulated result of Fovmod [6], and the row-planted model can be considered as a special case of CCM. Fig. 12(c) shows the similar characteristics of continuous crop because the row features of different directions will cancel each other out.

VI. CONCLUSION AND DISCUSSION

A new geometric optical model aimed at modeling the DBT distribution over mixed scenes of crop and road has been proposed in this letter. A typical mixed scene of 90×90 m^2 was used as a case study. One track of the WiDAS was selected for validation. The validation results indicate that the RMSE between the modeled results of the CCM and the airborne results is equal to 1.1 K, and the trends are very similar. If we use 4SAIL for simulation, the RMSE is also equal to 1.1 K. However, the trends of 4SAIL and WiDAS are obviously different because the effect of the road zone was not considered.

The row-planted and continuous canopy DBT model can be considered as two special cases of CCM through the sensitivity analysis. The limitations of this model include the following points: the multiscatter effects within the crop zone and between the crop side and the road are ignored; the pore of the vegetation side is ignored, and the camera calibration error and the atmospheric correction error are the error sources of our work. These errors will be thoroughly analyzed in the near future. The CCM requires that the crop area be continuous; the DBT distribution of mixed scenes of sparse crop and road will be discussed in the near future.

REFERENCES

[1] M. C. Anderson *et al.*, "A thermal-based remote sensing technique for routine mapping of land-surface carbon, water and energy fluxes from field to regional scales," *Remote Sens. Environ.*, vol. 112, no. 12, pp. 4227–4241, Dec. 2008.
[2] Z.-L. Li *et al.*, "Satellite-derived land surface temperature: Current status and perspectives," *Remote Sens. Environ.*, vol. 131, no. 15, pp. 14–37, Apr. 2013.
[3] H. Li *et al.*, "Evaluation of the VIIRS and MODIS LST products in an arid area of Northwest China," *Remote Sens. Environ.*, vol. 142, pp. 111–121, Feb. 2014.
[4] Y. M. Du, Q. H. Liu, L. F. Chen, Q. Liu, and T. Yu, "Modeling directional brightness temperature of the winter wheat canopy at the ear stage," *IEEE Trans. Geosci. Remote Sens.*, vol. 45, no. 11, pp. 3721–3739, Nov. 2007.
[5] J. P. Lagouarde *et al.*, "Modelling daytime thermal infrared directional anisotropy over Toulouse city centre," *Remote Sens. Environ.*, vol. 114, no. 1, pp. 87–105, Jan. 15, 2010.
[6] H. Ren *et al.*, "Impact of sensor footprint on measurement of directional brightness temperature of row crop canopies," *Remote Sens. Environ.*, vol. 134, pp. 135–151, Jul. 2013.
[7] J. A. Sobrino and J. Cuenca, "Angular variation of thermal infrared emissivity for some natural surfaces from experimental measurements," *Appl. Opt.*, vol. 38, no. 18, pp. 3931–3936, Jun. 20, 1999.
[8] X. Li *et al.*, "Heihe Watershed Allied Telemetry Experimental Research (HiWATER): Scientific objectives and experimental design," *Bull. Amer. Meteorol. Soc.*, vol. 94, no. 8, pp. 1145–1160, Aug. 2013.
[9] Q. Xiao and J. Wen, "HiWATER: Wide-angle infrared dual-mode line/area array scanner, WIDAS (3th, August, 2012)," Heihe Plan Science Data Center, Heihe, China, 2013.
[10] W. Verhoef, L. Jia, Q. Xiao, and Z. Su, "Unified optical-thermal four-stream radiative transfer theory for homogeneous vegetation canopies," *IEEE Trans. Geosci. Remote Sens.*, vol. 45, no. 6, pp. 1808–1822, Jun. 2007.
[11] B. Y. Yan, X. R. Xu, and W. J. Fan, "A unified canopy bidirectional reflectance (BRDF) model for row ceops," *Sci. China Earth Sci.*, vol. 55, no. 5, pp. 824–836, May 2012.
[12] D. S. Kimes, "Remote-sensing of row crop structure and component temperatures using directional radiometric temperatures and inversion techniques," *Remote Sens. Environ.*, vol. 13, no. 1, pp. 33–55, Mar. 1983.
[13] H. G. Huang, Q. Liu, Q. H. Liu, and W. H. Qin, "Validating theoretical simulations of thermal emission hot spot effects on maize canopies," *Int. J. Remote Sens.*, vol. 33, no. 3, pp. 746–761, Feb. 2012.
[14] L. F. Chen and Q. H. Liu, "The thermal radiant directionality of continuous vegetation," *J. Remote Sens.*, vol. 5, pp. 407–415, 2001, Chinese.